doi: 10.4149/gpb_2022063

BST-1 aggravates aldosterone-induced cardiac hypertrophy *via* the Ca^{2+}/CaN/NFATc3 pathway

Yao Yuan[1], Lina Zhao[1,2], Hongjuan Cao[1], Sha Li[1,2], Chunyan Liao[1,2], Lei Fu[1,2], Xing Wang[1], Fuqin Huang[1], Weidan Zeng[1], Aiyue Li[1] and Bei Zhang[1,2]

[1] *Guizhou Medical University, Guiyang, Guizhou, China*
[2] *Department of Ultrasound Center, The Affiliated Hospital of Guizhou Medical University, Guiyang, Guizhou, China*

Abstract. BST-1 (bone marrow stromal cell antigen-1) is thought to be a key molecule involved in regulating the functional activity of cells in various tissues and organs. BST-1 can catalyze the hydrolysis of nicotinamide adenine dinucleotide (NAD^+) to produce cyclic ADP ribose (cADPR), which activates the activity of intracellular Ca^{2+} signaling. Currently, the role of BST-1 regulation of Ca^{2+} signaling pathway in pathological myocardial hypertrophy is unclear. We found elevated expression of BST-1 in cardiac hypertrophy tissues of spontaneously hypertensive rats in our *vivo* study, subsequently; the mechanism of BST-1 action on myocardial hypertrophy was explored *in vitro* experiment. We used aldosterone (ALD) to induce H9C2 cellular hypertrophy. cADPR levels and intracellular Ca^{2+} concentrations declined and calcium-regulated neurophosphatase (CaN) activity and protein expression were decreased after BST-1 knockdown. And then activated T-cell nuclear factor (NFATc3) entry nucleus was inhibited. All of the above resulted in that H9C2 cells size was reduced by rhodamine-phalloidin staining. Thus, BST-1 may exacerbate cardiac hypertrophy by activating the Ca^{2+}/CaN/NFATc3 pathway.

Key words: BST-1 — Cardiac hypertrophy — CaN — NFATc3 — Aldosterone

Abbreviations: ALD, aldosterone; BST-1, bone marrow stromal cell antigen-1; cADPR, cyclic ADP ribose; CaN, calcineurin; NAD^+, nicotinamide adenine dinucleotide; NFATc3, activated nuclear factor of T cell; RAAS, renin-angiotensin-aldosterone system.

Introduction

Many cardiovascular diseases are characterized by cardiac hypertrophy (Koitabashi and Kass 2011; Zeitz and Smyth 2020). Increased cardiac contractility results from hypertrophy, which is as formed as a benign, adaptive response to physiological and pathological stress. The complex process that ultimately leads to heart failure along with cardiac remodeling and dysfunction is caused by chronic stimulation, which causes hypertrophy to change into pathologic hypertrophy (Nakamura and Sadoshima 2018; Oldfield et al. 2020). The pathogenesis of cardiac hypertrophy, which includes elevated myocardial afterload, renin-angiotensin-aldosterone system (RAAS) activation, cardiomyocytes death, and increased sympathetic nerve excitability, is currently not completely investigated (Tham et al. 2015; Oldfield et al. 2020; Takano et al. 2020). The synthesis of renin, angiotensin, and aldosterone (ALD), which cause myocardium hypertrophy, fibrosis, and cardiac remodeling, are caused by the long-term activation of RAAS (Raman et al. 1995; Somanna et al. 2015). However, there are currently no known medications that can successfully reverse the abnormal cardiac hypertrophy and reduce the morbidity and mortality associated with heart failure. Therefore, identifying novel therapeutic targets may result from the discovery of novel molecular mechanisms of cardiac hypertrophy.

Correspondence to: Bei Zhang, NO. 28 Guiyi street, Yunyan District, Guiyang 550004, China
E-mail: zhangbei@gmc.edu.cn

Myocardial hypertrophy development is substantially related to Ca^{2+}-induced signaling pathways (Frey et al. 2000; Berridge et al. 2006) . When stimulated by the inward flow of extracellular Ca^{2+} or the release of intracellular calcium pools, cADPR functions as a second messenger for intracellular Ca^{2+} activity, leading to a rise in cytoplasmic Ca^{2+} concentration in cardiomyocytes (Lee et al. 1991; Higashida et al. 1999). Ca^{2+} binds to the regulatory subunit of calcineurin (CaN), boosting the activity of CaN (Kakalis et al. 1995; Li et al. 2011). The CaN/NFAT (activated nuclear factor of T cell) pathway is then successfully turned on after that. NFAT has an N-terminal regulatory domain, which is phosphorylated in unstimulated cells, and CaN dephosphorylate NFAT into the nucleus after the cell is stimulated. NFAT will move back from the nucleus to the cytosol under the control of NFAT kinase and stop the regulation of gene transcription when the cytosolic Ca^{2+} concentration declines (Li et al. 2011).

BST-1/CD157 (bone marrow stromal antigen-1), a glycoprotein that is glycosylphosphatidylinositol (GPI)-anchored and encoded by the members of the NAD^+ hydrolase/ADP cyclase gene family (Ortolan et al. 2002; Malavasi et al. 2008). It participates in a number of cellular processes, such as humoral immunity and leukocyte trafficking, and carries out some signal transduction as an extracellular enzyme and signaling receptor (Ishihara et al. 2000; Morone et al. 2014). Jing Li et al. found that upregulating BST-1 on bone marrow mesenchymal stem cells in spinal cord damaged rats induced mitochondrial transferring from bone marrow mesenchymal stem cells to damaged cells by increasing cADPR levels, thereby promoting neural regeneration and apoptosis (Li et al. 2021). Additionally, it has been reported that BST-1 has an activity of NAD^+ hydrolase since it can convert the majority of NAD^+ into cADPR (Hirata et al. 1994; Yamamoto-Katayama et al. 2002). However, few studies have examined role of BST-1 in the heart. Our studies showed that BST-1 is existed in the heart and activated in the hypertrophic myocardium of spontaneous hypertension rats. Therefore, we hypothesize that BST-1 participates in the process of cardiac hypertrophy formation *via* the Ca^{2+}/CaN/NFAT signaling pathway.

Materials and Methods

Animals

All animal experiments were carried out in line with Guizhou Medical University Institutional Animal Care and Use Committee (Guizhou, China). The Ethics Committee (CEUA) No.1900572 approved the experimental methodology, and 9-week-old male Wister rats (250–300 g) and SHR rats (250–300 g) were bought from the Guizhou Medical University Animal Center. All rats were kept in housing with free access to food, water, and an environment with controlled temperature (23–24°C) and relative humidity (50–60%). Regular measurements of the rat's body weight were taken. At 26 weeks, the rats were euthanized, and their blood and hearts were collected for subsequent analyses.

Blood pressure measurement and echocardiography

Systolic blood pressure (SBP) and diastolic blood pressure (DBP) were assessed on a regular basis in the tails of conscious rats using a noninvasive computerized tailcuf system (Kent Scientifc Corporation, CT, USA). Each rat was placed in a heated tube (38°C) for 10–15 min, after which its body temperature was monitored to increase. Each rat was measured three times, and each set of rats was measured concurrently. The value of this parameter for the animal was determined by averaging these three values. Echocardiographic examinations in various age groups were used to track the development of myocardial hypertrophy. Transthoracic 2-dimensional (2D), M-mode and Doppler echocardiographic studies were performed with Mylab50 (Esaote, Italy) using a high-resolution transducer (SL3116) with frequency of 22 MHz.

Cell culture and treatment

H9c2(2-1) rat cardiomyocytes were obtained from ATCC (American Type Culture Collection). H9c2 cells were cultured using Gibco high glycemic medium (DMEM) supplemented with 10% fetal bovine serum (FBS). Cells were grown in a humidified incubator containing 5% CO_2 at 37°C. We used ALD (Sigma, USA) to induce the hypertrophy of H9C2 based on earlier publications in the literature and our preliminary studies.

Histopathological studies

Araffin-embedded fixed heart tissues were then cut into 5-μm-thick sections. Changes in myocardial structure were assessed by hematoxylin-eosin (HE) staining (Solarbio, China). The degree of fibrosis was evaluated using a Masson staining kit (Solarbio, China). Micrographs were taken with a microscope (Olympus VS200, JPN). The percentage of collagen stained area (blue) was calculated using a quantitative digital image analysis system (ImageJ 1.47 software, NIH).

Cell viability assay

Cell viability was measured by CCK8 method (Tong Ren, China). Briefly, H9C2 cells were treated with ALD at concentrations of 10^{-7}, 10^{-6}, 10^{-5}, 10^{-4} and 10^{-3} mol/l for 48 h. After that,10 μl of CCK-8 solution was added to each well and incubated at 37°C for 2 h; then, the OD (optical density) value for each well was read at wavelength 450 nm

with a microplate reader (Thermo, USA). The assay was repeated 3 times. The cell viability was calculated as follows: cell viability (%) = [OD (experiment) – OD (blank)] / [OD (control) – OD (blank)] × 100.

RNA interference

siRNAs for BST-1 and negative control (siRNA-NC) were ordered from Shanghai Biotech Co. (Shanghai, China), there are three sequences of rat BST-1 targeting SiRNA. Synthesis and selection of siRNA for BST-1: BST-1-SiRNA#1:(sense 5'-UCAAGGUGGUGCUGGACAATT-3', antisense 5'-UUGUCCAGCACCACCUUGATT-3'); BST-1-SiRNA#2: (sense 5'-GUGGAUGCCUAUUGGAAAATT-3', antisense 5'-UUUUCCAAUAGGCAUCCACTT-3'); BST-1-SiRNA#3: (sense 5'-GGAAAAUGCCUCUGGACUUTT-3', antisense 5'-AAGUCCAGAGGCAUUUUCCTT-3').

Transfections of the siRNAs were performed by using LipofectamineTM 2000 (Thermo Fisher Scientific, USA) according to the manufacturer's protocol. Briefly, H9C2 cells were seeded in 6-well plates to obtain approximately 40–50% confluence. 500 μl of mixture containing siRNA (100 nM for each) and transfection reagents (6 μl for each) were added to the cells for 6 h at 37°C and then replaced with fresh culture medium. H9c2 cells were incubated at 37°C for 48 h. The knockdown efficiency was confirmed by qRT-PCR and Western blotting, and the sequence with the highest knockdown efficiency was selected, and experiments were performed.

Rhodamine-phalloidin staining

To assess changes in H9C2 hypertrophy, cells were fixed with 4% paraformaldehyde, treated for 1 h at room temperature in accordance with the instructions of the Rhodamine-phalloidin staining kit (Beyotime, China), and then blocked with an anti-fluorescence quencher containing DAPI (Solarbio, China). A fluorescent microscope was used to find immunofluorescence in the cells (Olympus VS200, JPN).

Immunofluorescence

Cell crawlers covering 6-well culture plates were covered in H9C2 cells. Briefly, the cells were then sealed with 10% goat serum at 37°C for 1 h after being placed in 4% paraformaldehyde, 0.1% TritonX 100 for 20 min, and 0.1% TritonX 100 for permeabilization. After that, the cells were incubated with rabbit, anti-BST-1 and anti-NFATc3 primary antibody for an overnight incubation at 4°C. Cells were then washed three times with PBS, incubated with goat anti-rabbit Cy3-labled antibody for 1 h at room temperature, and the slices were sealed with DAPI-containing anti-fluorescence quenching blocker. Under a fluorescent microscope, immunofluorescence analysis was carried out (Olympus VS200).

Ca^{2+} fluorescence measurement

We bought Fluo3am from Solarbio (China). Cultured cardiomyocytes H9C2 were treated for 20 min at 37°C in the dark with a working solution of Fluo3am (5 μM) containing 0.03% Pluronic F-127. Then, HBSS containing 1% serum was multiplied five times and incubated for 40 min at 37°C. HEPES underwent three washings. Then, using a fluorescent microscope (Olympus VS200) with an excitation wavelength of 488 nm and an emission wavelength of 530 nm, the fluorescence intensity of intracellular Ca^{2+} was captured.

Measurement of serum biomarker levels

According to the experimental protocols, myocardial tissue and H9C2 cells samples were removed for examination of lactate dehydrogenase (LDH) activity to determine the severity of myocardial injury (Nanjing Jiancheng, China).

Western blotting

Protein lysates from cells and heart tissue were separated using 10% sodium dodecyl sulfate-polyacrylamidegel electrophoresis (SDS-PAGE) and then electrically transferred to PVDF membranes (Millipore, USA). Each membrane was first preincubated for 1 h in closure buffer (TBST with 5% skim milk) before being incubated with the appropriate primary anti-body overnight at 4°C. The anti-BST-1 antibody (Thermo Fisher Scientific, USA), the anti-CaN antibody (PTMab, China), the anti-NFATc3 antibody (Proteintech, China), the anti-Lamin B1 antibody (Proteintech, China), the anti-β-actin antibody (Genetex, USA). The membranes were then exposed by using a Tanon 5200 chemiluminescence apparatus after being treated with a secondary antibody (Neobioscience, China) for 1 h at room temperature. Using ImageJ software (ImageJ 1.47 software, USA), the data were evaluated and processed as relative optical density (ROD, relative to β-actin).

Quantitative real-time RT-PCR (qRT-PCR)

Total RNA from H9C2 cells was extracted using the Trizol technique (Sigma-Aldrich, USA). The YESEN kit reverse transcribed cDNA. The SYBR Green Master Mix (YESEN, China) and the iCyclerIQ equipment were used to perform qRT-PCR (BioRad, USA). qRT-PCR was performed in an initial denaturation step at 95°C for an initial denaturation step of 2 min, and 40 cycles in 95°C/10 s and 60°C/30 s. The amount of endogenous control (β-actin) was used to standardize the expression of the mRNA. The primers targeting the genes were as follows: BST-1: forward 5'-GTACCACGCCTCACCTCCAGAG-3', reverse 5'-CCTTGTCCAGCACCACCTTGAAG-3'; ANP: for-

ward 5'-GAGAGTGAGCCGAGACAGCAAAC-3', reverse 5'-GAAGAAGCCCTTGGTGATGGAGAAG-3'; BNP: forward 5'-CCAGTCTCCAGAACAATCCACGATG-3', reverse 5'-GCCTTGGTCCTTTGAGAGCTGTC-3'; Myh7: forward 5'-CACCAGCCTCATCAACCAGAAGAAG-3', reverse 5'-TCCTCTGCGTTCCTACACTCCTG-3'; β-actin: forward 5'-TGTCACCAACTGGGACGATA-3', reverse 5'-GGGGTGTTGAAGGTCTCAAA-3'

Statistical analysis

All results are shown as means ± standard deviation (SD) and were analyzed using SPSS (SPSS 23.0) from at least three independent experiments. Two-tailed unpaired Student's *t*-test was used for analyzing the comparison between the two groups and one-way ANOVA was used for analyzing the comparison among multiple groups. When $p < 0.05$, the data were considered to be statistically significant.

Results

BST-1 expression was upregulated in spontaneously hypertensive rats' hypertrophic myocardium

In vivo experiments, we established a rat model of cardiac hypertrophy by using spontaneously hypertensive rats (SHR), and we assessed the cardiac function of the rats by using echocardiography. The blood pressure of the rats increased with increasing week age gradually, and maintained at SBP of about 200 mmHg after reaching the age of 18 weeks (Fig. 1A). In comparison to Wistar rats (WT) group, the SHR at an age of 26 weeks displayed a significant increase in interventricular septal thickness, a decrease in ejection fraction (LVEF%), a decrease in shortening fraction (LVFS%), a decrease in left ventricular diastolic diameter (LVIDD), and an increase in interventricular septal thickness (IVSD), as seen in Figure 1B. Subsequently, we executed the rats and weighed their hearts after lavage. In contrast to the WT group, the SHR group heart weight/body weight (HW/BW) increased (Fig. 1C), cardiomyocytes volume was increased and the cell arrangement was disturbed by HE staining, the blue collagen deposits were visible in the myocardial interstitium by Masson staining (Fig. 1D), and collagen area% was increased (Fig. 1E). The extent of myocardial damage was then determined by measuring myocardial enzyme activity, and as can be seen in Figure 1F, LDH enzyme activity – a sign of myocardial damage – was elevated in the SHR group. These had shown that the myocardium of SHR, which would be used in subsequent experiments, had suffered pathological hypertrophic changes. Next, our studies showed that SHR heart tissues had higher levels of BST-1 mRNA and protein in comparison to the WT group (Fig. 1G,H).

BST-1 expression was increased in H9C2 hypertrophic cells with ALD treatment

We used ALD to induce H9C2 cellular hypertrophy *in vitro* experiments to investigate the role of BST-1 in cardiac hypertrophy. ALD, a member of the RAAS, affects the apoptosis, fibrosis, and myocardial hypertrophy of the heart. As a result, the cell size was increased with ALD treatment. First, H9C2 cells were exposured to 10^{-7},10^{-6},10^{-5},10^{-4} and 10^{-3} mol/l concentration of ALD treatment for 48 h individually. Figure 2A displayed the outcomes of the cell viability assay by using CCK8 kit. The cell viability was more appropriate than other conditions when H9c2 cells were treated with 10^{-5} mol/l concentration of ALD, and this concentration was used for following *vitro* experiments. BST-1 mRNA and protein expression levels rose with ALD treatment (Fig. 2B,C). These results were in agreement with the increase in BST-1 expression observed in hypertrophic SHR hearts. BST-1 is a cell surface glycoprotein which is consist of a single amino acid chain while the chain locates outside the cytomembrane (Ferrero et al. 2017). The immunofluorescence observed that the fluorescence intensity of BST-1 increased, and it was expressed in the cytoplasm and nucleus in H9C2 with ALD treatment (Fig. 2D).

Cardiac hypertrophy induced by aldosterone was inhibited following BST-1 knockdown

By transfecting three sequences of BST-1-SiRNAs #1, #2, and #3, we were able to knockdown BST-1. The efficiency of transfection was confirmed by qRT-PCR and Western blotting. BST-1-SiRNA#3 was knocked down the most effectively, as seen in Figure 3A and B, and following experiments made advantage of this SiRNA sequence. Next, we used Rhodamine-phalloidin staining to assess the degree of H9C2 cellular hypertrophy. The surface area of H9C2 cells expanded with ALD treatment, whereas the surface area of H9C2 cells transfected with BST-1-SiRNA decreased (Fig. 3C). We used qRT-PCR to measure the mRNA levels of the cardiac hypertrophy markers in four groups of cardiomyocytes, including atrial natriuretic peptide (ANP), brain natriuretic peptide (BNP), and beta-myosin heavy chain(myh7) (Potter et al. 2004). As shown in Figure 3D, we observed that the mRNA expression of ANP, BNP, and myh7 were decreased following BST-1 knockdown in comparison to its negative control group (ALD+Si-NC). In order to evaluate for cardiomyocyte injury, we also measured LDH activity in the four groups of cells. The results revealed that LDH activity was higher in the ALD group than in the NC group; however, BST-1 knockdown suppressed it (Fig. 3E). These findings supported a role for BST-1 in the pathological cardiac hypertrophy by showing that BST-1 expression was markedly elevated in hypertrophic heart tissues and cardiomyocytes.

BST-1 activated Ca^{2+} signaling by increasing the levels of cADPR

It has been demonstrated that BST-1 displays NAD^+ hydrolase capability. One of the products of this hydrolysis is cADPR, which plays an important role in Ca^{2+} activity and cardiac excitation-contraction coupling. We measured cADPR levels and intracellular Ca^{2+} concentration *in vitro* experiments to explore whether that BST-1 impacted cardiac hypertrophy by hydrolyzing NAD^+. As seen in Figure

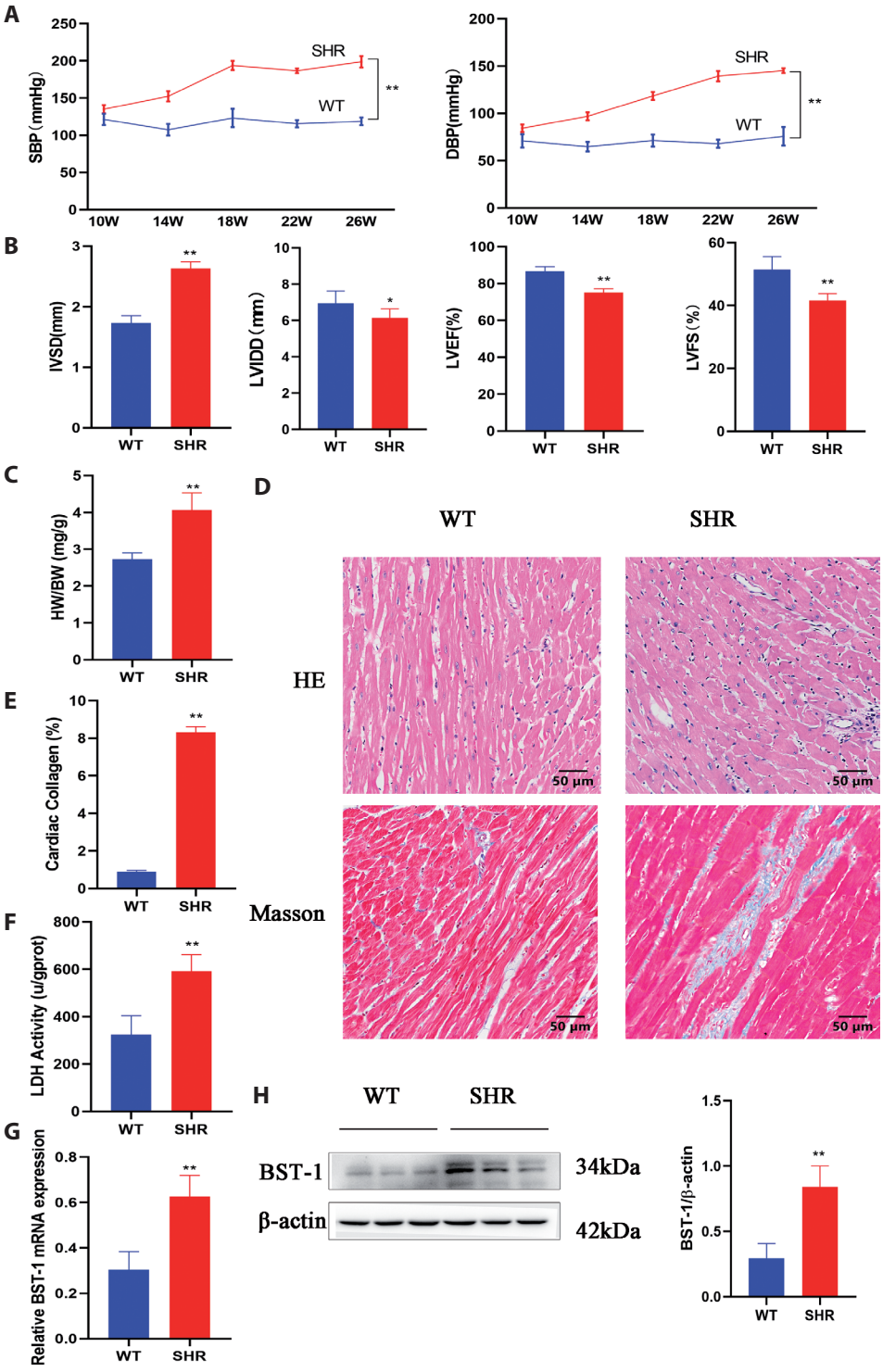

Figure 1. BST-1 expression was upregulated in spontaneously hypertensive rats (SHR) hypertrophic myocardium. **A.** Systolic blood pressure (SBP) and diastolic blood pressure (DBP) in Wistar rats (WT) and SHR groups. **B.** Echocardiography of WT and SHR at 26 weeks of the age. **C.** HW/BW (heart weight/body weight). **D.** HE and Masson staining of myocardial cross-sections in WT and SHR groups (scale bar = 50 μm). **E.** Quantification of cardiac collagen (%) from Masson staining. **F.** Lactate dehydrogenase (LDH) enzyme activity of rat myocardial tissues. **G.** qRT-PCR to detect the mRNA levels of BST-1 in WT and SHR groups. **H.** The protein expression levels of BST-1 in WT and SHR groups were determined by Western blotting. * $p < 0.05$, ** $p < 0.01$ *vs.* WT group. $n = 6$ *per* group. IVSD, interventricular septal thickness at diastole; LVIDD, left ventricular diastolic diameter; LVEF%, ejection fraction; LVFS%, shortening fraction; w, week.

4A, cADPR levels in H9C2 rose with ALD treatment and decreased by BST-1-SiRNA transfection. Fluo-3am fluorescence showed that Ca^{2+} fluorescence intensity in H9C2 cells increased with ALD treatment and decreased after BST-1 knockdown (Fig. 4B,C). According to the aforementioned studies, cADPR and Ca^{2+} were probably implicated in cardiomyocyte hypertrophy, and the influence of BST-1 on myocardial hypertrophy was achieved by raising the levels of cADPR.

The effect of BST-1 on cardiac hypertrophy was dependent on the CaN/NFATc3 pathway

The CaN/NFATc3 signaling pathway has been demonstrated to be one important pathway regulated by Ca^{2+} among those that have been linked to the development of myocardial hypertrophy, according to a substantial amount of literature. We wanted to confirm whether the CaN/NFATc3 signaling pathway was the mechanism by which BST-1 affected myocardial hypertrophy. We measured the enzymatic activity and protein expression levels of CaN *in vitro* experiments. Figure 5A and B illustrated how ALD treatment increased CaN enzymatic protein expression levels and activity in H9C2 cells, while BST-1-SiRNA transfection decreased CaN enzymatic protein expression levels and activity. The N-terminal regulatory domain of NFAT regulates its nuclear input when CaN is activated. This regulatory domain is phosphorylated in unstimulated cells, which obscures the nuclear localization sequence and causes the NFAT protein to be isolated in the cytoplasm. The NFAT regulatory structural domain is

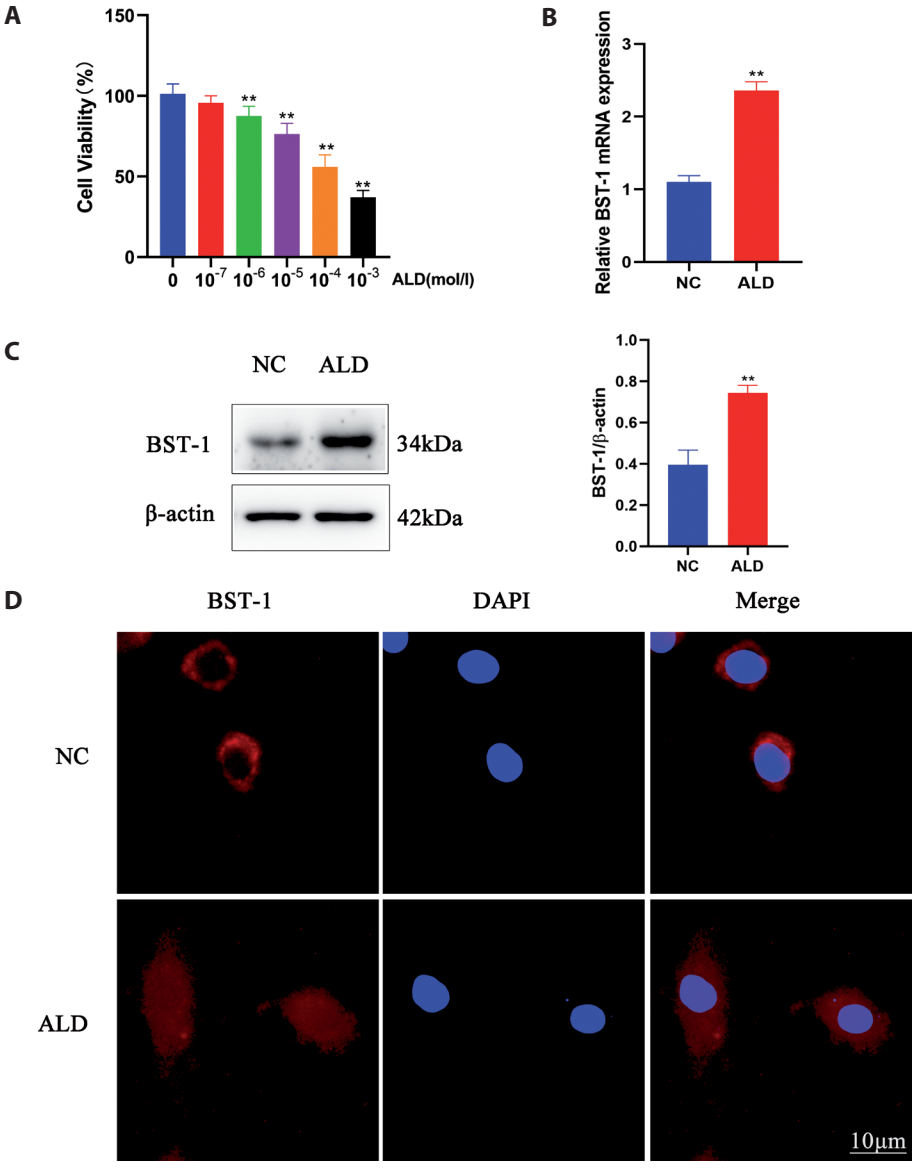

Figure 2. BST-1 expression was increased in H9c2 hypertrophic cells with aldosterone (ALD) treatment. **A.** CCK8 detected the survival rate of H9c2 cells treated with 10^{-7},10^{-6},10^{-5},10^{-4} and 10^{-3} mol/l concentration of ALD for 48 h. ** $p < 0.01$ *vs.* 0 mol/l ALD. **B.** BST-1 mRNA expression levels in the ALD group in comparison to the NC group by qRT-PCR. ** $p < 0.01$ *vs.* NC. **C.** BST-1 protein expression levels in *in vitro* tests in the ALD group and NC group by Western blotting. ** $p < 0.01$ *vs.* NC. **D.** The expression of BST-1 (stained in red) was determined using an immunofluorescence assay. Nucleus was stained with DAPI (in blue). Scale bar = 10 μm. All data were obtained from three independent experiments. NC, negative control. (See online version for color figure.)

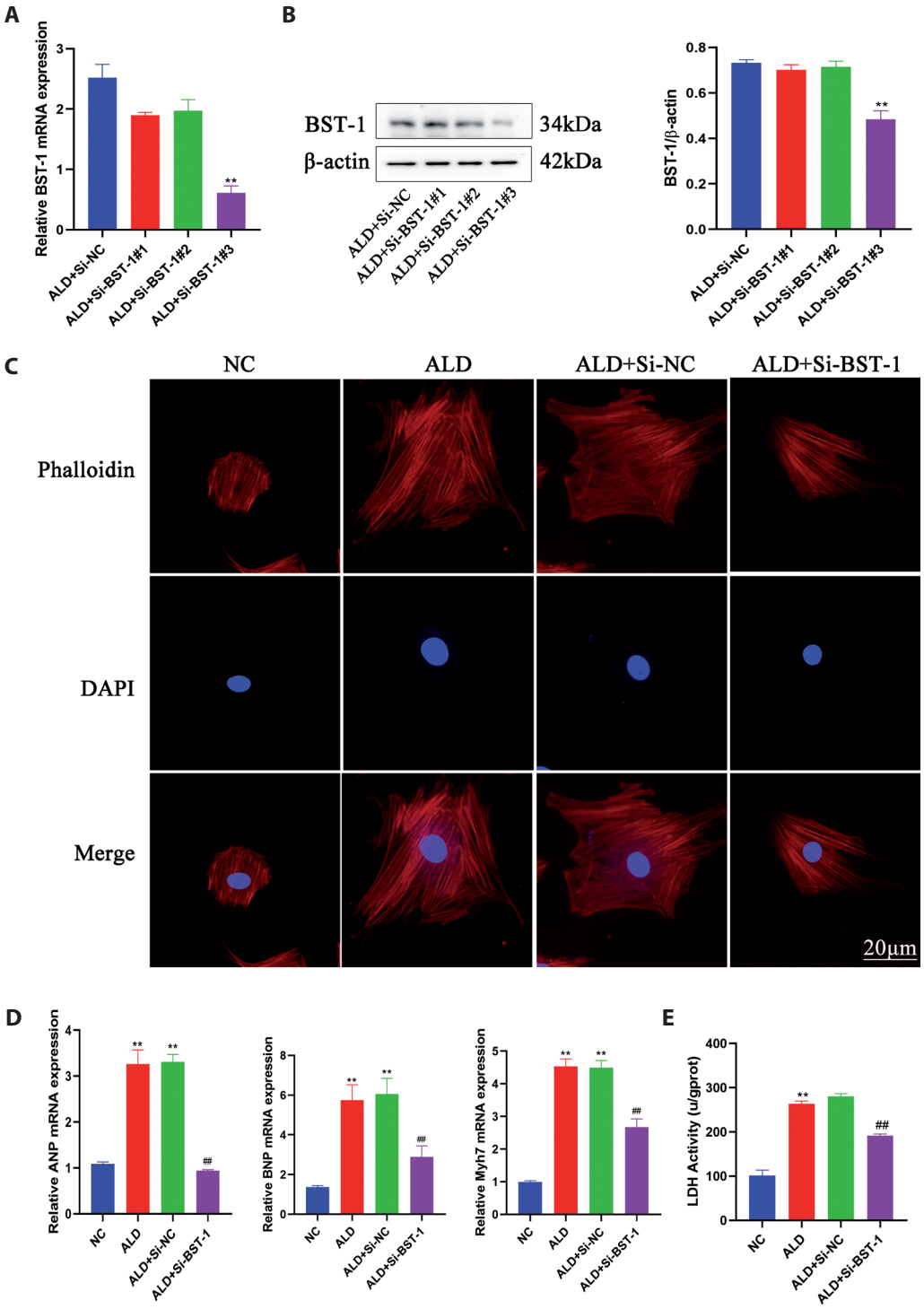

Figure 3. Cardiac hypertrophy induced by aldosterone (ALD) was inhibited following BST-1 knockdown. **A.** BST-1 was knockdown by using three siRNA sequences while being subjected to an ALD treatment, and qRT-PCR was used to measure BST-1 mRNA levels. ** $p < 0.01$ *vs.* ALD+Si-NC. **B.** Western blotting was used to confirm the protein levels of BST-1. ** $p < 0.01$ *vs.* ALD+Si-NC. **C.** H9c2 cytoskeleton was stained with Rhodamine-phalloidin staining. Cell surface area was represented in red fluorescence area, and nucleus was shown with DAPI in blue. Scale bar = 20 μm. **D.** ANP, BNP, and Myh7 mRNA expression levels in the four H9c2 groups by qRT-PCR. ** $p < 0.01$ *vs.* NC, ## $p < 0.01$ *vs.* ALD+Si-NC. **E.** Lactate dehydrogenase (LDH) activity testing, which measures a cardiac enzyme indicative of myocardial damage. ** $p < 0.01$ *vs.* NC, ## $p < 0.01$ *vs.* ALD+Si-NC. All data were obtained from three independent experiments. NC, negative control.

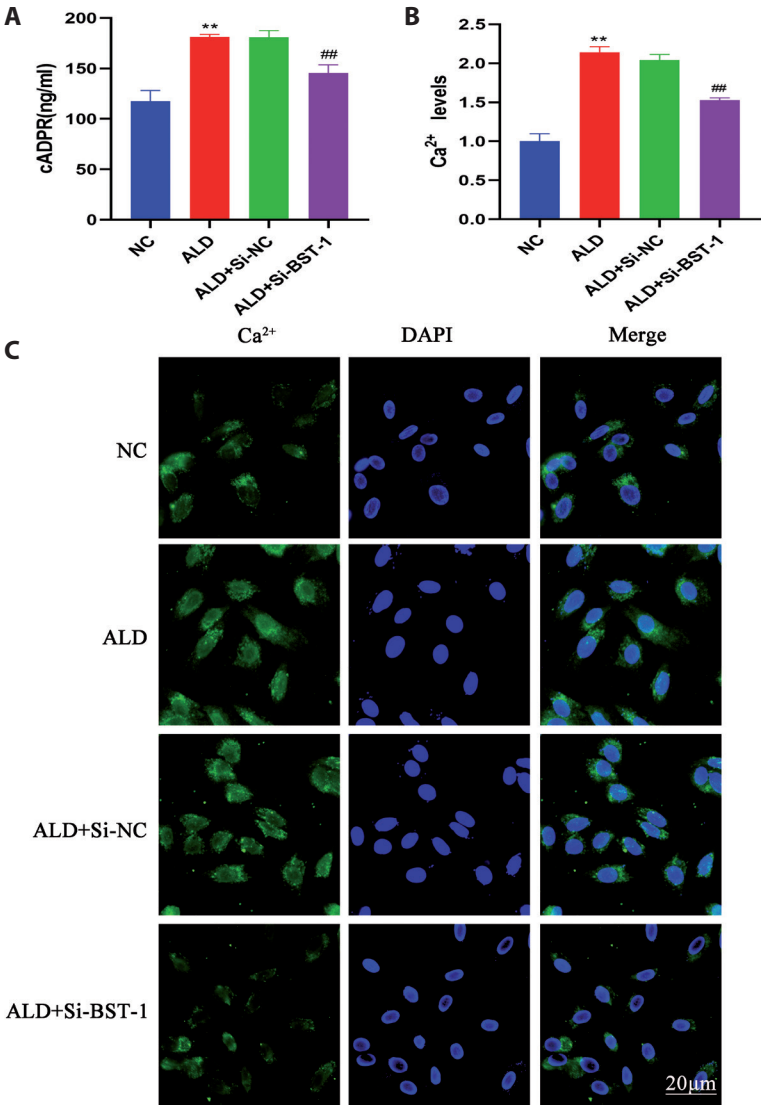

Figure 4. BST-1 activated Ca^{2+} signaling by increasing cADPR levels. **A.** The levels of cADPR, a result of NAD^+ hydrolysis, in four groups of H9c2 cells. **B., C.** Fluo-3am measurement of the Ca^{2+} concentration in four groups of H9c2 cells. Fluorescently labeled Ca^{2+} was shown in green, and DAPI-stained nucleus was shown in blue. Statistical quantitative analysis of the Ca^{2+} fluorescence intensity (B). Scale bar = 20 μm. All data were obtained from three independent experiments. $^{**}p < 0.01$ *vs.* NC, $^{\#\#}p < 0.01$ *vs.* ALD+Si-NC. For abbreviations, see Figure 3. (See online version for color figure.)

dephosphorylated by CaN activation, which leads to a change in the protein conformation and enables NFAT translocation into the nucleus. NFATc3 was found to be in the cytoplasm in the NC group, but with ALD treatment, it entered the nucleus; this entry was then inhibited by transfection with BST-1-SiRNA (Fig. 5C). While this was going on, we isolated nuclear proteins from four different groups of, and Western blotting analysis showed that the expression of the protein NFATc3 in the nucleus of H9C2 cells increased with ALD treatment and decreased following BST-1 knockdown (Fig. 5D).

Discussion

An independent risk factor for an increased prevalence of various cardiovascular illnesses and death is pathological cardiac hypertrophy. Pathological myocardial hypertrophy can be brought on by a variety of mechanisms, including elevated anterior and posterior stress on the myocardium, activation of the sympathetic nervous system, and activation of the RAAS system (Yamazaki et al. 1999; Finckenberg et al. 2010; Samak et al. 2016; Nakamura et al. 2017). Chronic hypertension results in a persistent buildup of pressure inside the heart, which induces adaptive cardiac remodeling. This pathological myocardial hypertrophy finally causes heart failure (Johnson et al. 1996). The blood pressure of SHR rise with age and finally maintain a systolic blood pressure above 200 mmHg. SHR have a hereditary background of hypertension that is similar with the evolution of primary hypertensive illness in humans (Doris et al. 2017). We chose SHR as an animal model of chronic pressure overload resulting to myocardial hypertrophy because chronic cardiac

pressure overload increases the production of cardiac structural proteins, increases left ventricular mass, thickens the wall, and causes myocardial interstitial fibrosis (Holjak et al. 2022). Our echocardiogram showed that, when compared to WT group, SHR at 26 weeks of age had considerably thicker septal and posterior left ventricular walls and worse cardiac function. In comparison to the WT group, the SHR group HW/BW increased. Masson staining revealed blue collagen deposits in the myocardium interstitium, whereas HE staining in the SHR group revealed perturbed myocardial cell organization and increased cell volume. These showed SHR to have pathologically hypertrophic myocardium alterations. Increased ALD in the RAAS system intensifies catecholamine-induced cardiac injury and water-sodium retention. Additionally, it binds to the mineralocorticoid receptor, motivates cardiac cells to express fibrosis genes, boosts collagen production, and results in myocardial hypertrophy (Azibani et al. 2013). As a result, we conducted vitro experiments in this study to induce H9C2 cells hypertrophy by using ALD. In Rhodamine-phalloidin staining, it showed that the volume

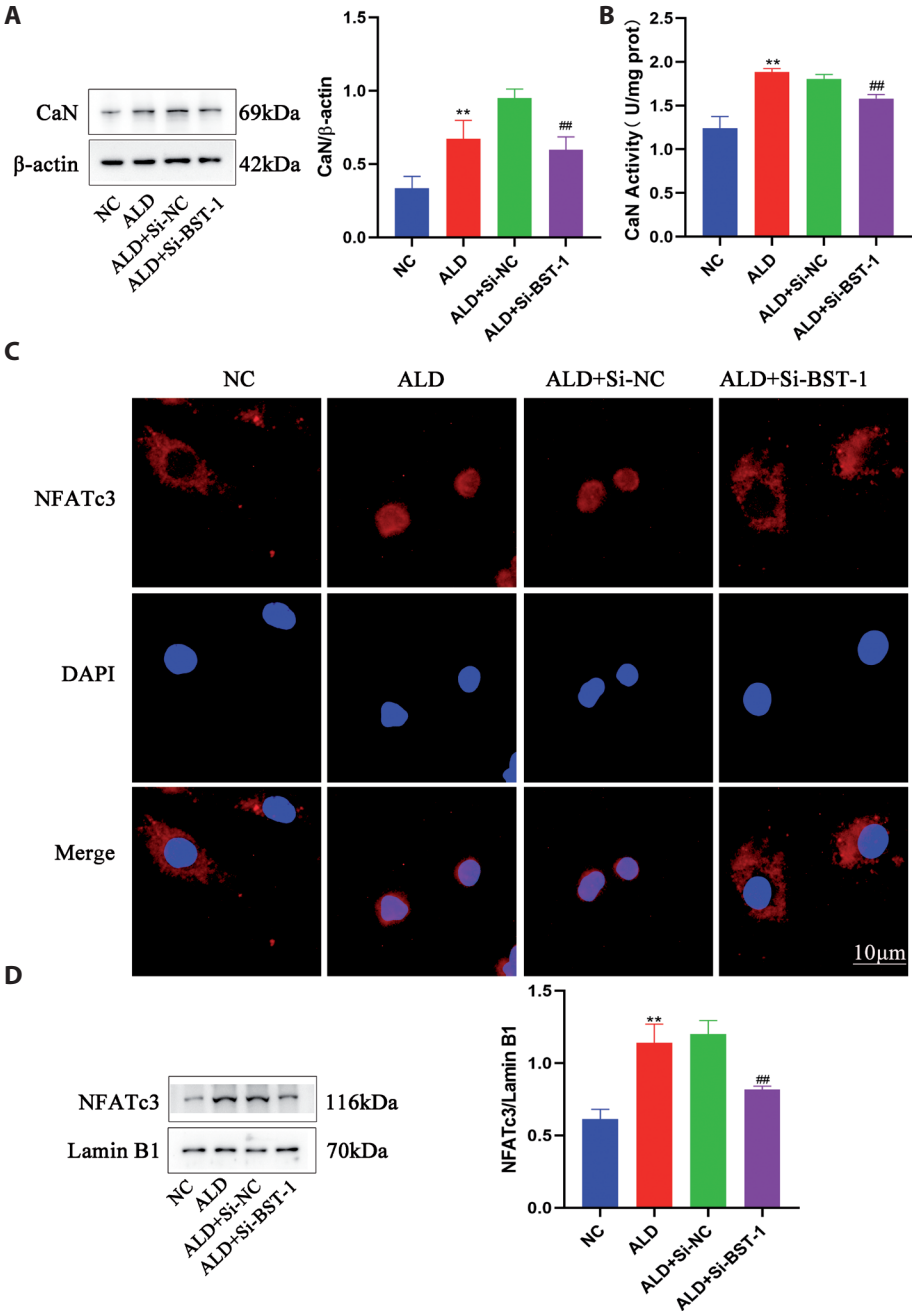

Figure 5. The effect of BST-1 on cardiac hypertrophy was dependent on the CaN/NFATc3 pathway. **A.** The proportions of H9c2 cells in four groups expressing CaN protein by Western blotting. **B.** The activity of the CaN enzyme in four groups of H9c2 cells. **C.** Immunofluorescence detection of NFATc3 expression in four groups of H9C2 cells. Red fluorescently labeled with NFATc3, nucleus stained with DAPI in blue. Scale bar = 10 μm. **D.** The levels of NFATc3 nuclear protein expression in four groups of H9c2 cells by Western blotting. The data were evaluated and processed as relative optical density (relative to Lamin B1). $^{**}p < 0.01$ *vs.* NC; $^{\#\#}p < 0.01$ *vs.* ALD+Si-NC. All data were obtained from three independent experiments. CaN, calcium-regulated neurophosphatase; NC, negative control; NFATc3, T-cell nuclear factor.

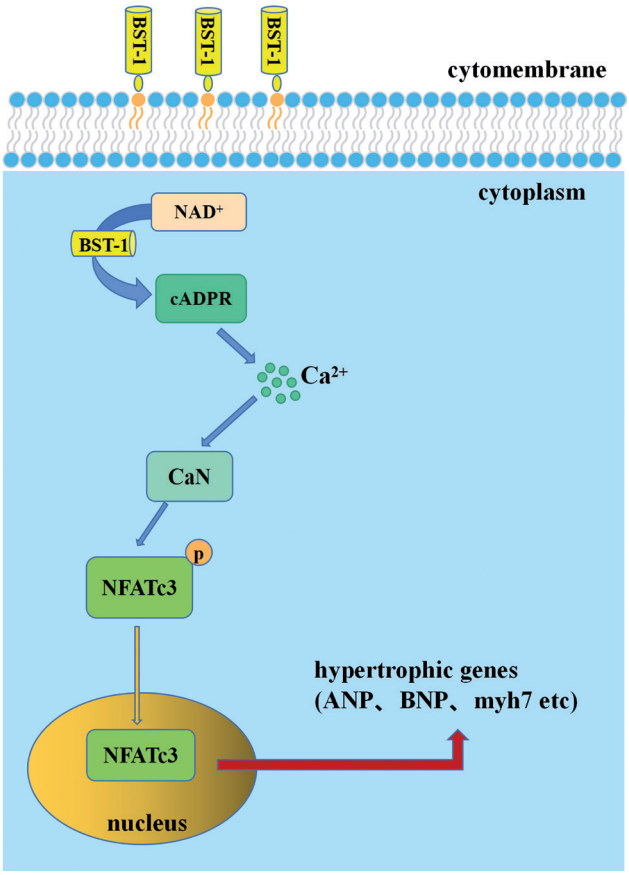

Figure 6. Diagrammatic illustration of BST-1 in cardiac hypertrophy. Upon cell stimulation in H9C2 cells, BST-1 can hydrolyze NAD^+ to produce cADPR. As an inducer of intracellular Ca^{2+} signaling, cADPR causes Ca^{2+} to be released from the intracellular calcium pool into the cytoplasm, further activating CaN. Then activated CaN dephosphorylates NFATc3 into the nucleus, and activates the transcription of genes associated with cardiac hypertrophy. For abbreviations, see Figure 5.

of H9C2 cells increased with ALD treatment in comparison to NC group. Myocardial hypertrophy indicators ANP, BNP, and myh7 mRNA expression increased. Additionally, LDH, the cardiac enzyme that was a hallmark of myocardial damage, displayed increased enzymatic activity. All of the above demonstrated that H9C2 cells charactered hypertrophy.

Cardiac hypertrophy progress is as a result of Ca^{2+}-mediated signaling pathways, the more common one is the CaN/NFAT signaling pathway (Zarain-Herzberg et al. 2011). A family of calcium-regulated transcription factors known as NFAT has a variety of functions in both development and illness (Molkentin et al. 1998). Four NFATc isoforms, NFATc1, NFATc2, NFATc3, and NFATc4 are present in ventricular cardiomyocytes (van Rooij et al. 2002). Activation of the CaN/NFATc3 pathway was promoted by the activation of transient receptor potential vanilloid acid (TRPV3) channels, which quickened the process of rat cardiac hypertrophy according to Zhang et al. (2018). The unique characteristic of NFAT is that Ca^{2+} and CaN control it. The phosphorylated NFAT, which is primarily located in the cell plasma at rest, is dephosphorylated by activated CaN and enters into nucleus. This causes transcription of genes related to cardiac hypertrophy and an increase in the production of cardiac fibroblast transfer growth factor (TGF-β), as well as an increase in the protein nucleic acid of cardiomyocytes. This results in an increase in the production of cardiomyocytes protein nucleic acids and larger cells, which causes abnormal cardiac hypertrophy to form. After cardiomyocytes are stimulated, the cytoplasmic Ca^{2+} concentration rises due to the inward flow of extracellular Ca^{2+} or the release of intracellular calcium pools. Then Ca^{2+} binds to the appropriate binding site with CaN, thereby activating the enzyme and triggering the CaN/NFAT cascade (Rao et al. 2009). According to research by Benitah et al., persistent aldosterone stimulation resulted in myocardial pathological remodeling by increasing calcium inward flow in cardiomyocytes, which eventually leaded to cardiac hypertrophy (Bénitah et al. 2001). This was further supported in our vitro studies by using H9C2 cells, which displayed increased intracellular Ca^{2+} concentrations and the activity and protein expression levels of CaN, and NFATc3 activating to enter into nucleus with ALD treatment.

In the current study, we first discovered BST-1 elevation in SHR hypertrophic cardiac tissues. However, its functional significance in the development of disease remains unclear. The following *in vitro* experiments explored this mechanism of BST-1. In ALD-induced H9C2 cells, it showed that BST-1 protein and mRNA levels were increased. This finding suggested that BST-1 could produce intracellular messengers in response to stimulate that catalyzed the synthesis of cADPR from NAD^+. Previous research demonstrated that after isoproterenol stimulation of mouse cardiomyocytes *in vitro* experiments, cADPR levels increased and cardiomyocytes displayed hypertrophic manifestations (Gul et al. 2016). cADPR is an important cytoplasmic messenger for Ca^{2+} actors. Our findings indicated that after ALD stimulation of H9C2 cells, intracellular cADPR levels similarly exhibited an increasing trend and Ca^{2+} concentration rose, activating the CaN/NFATc3 pathway to support cardiac hypertrophy. Additionally, BST-1 knockdown in ALD-induced hypertrophy of H9C2 cells lowered intracellular cADPR and Ca^{2+} levels, inhibited the CaN/NFATc3 pathway, and decreased cardiomyocyte hypertrophy. It implied that inhibiting BST-1 through Ca^{2+}/CaN/NFATc3 may reduce myocardial hypertrophy. The potential mechanisms by which stimulation of BST-1 worsen cardiac hypertrophy are summarized in Figure 6. Notably, the amino acid chain of BST-1 is positioned on the outside of the cytosolic membrane and is devoid of any transmembrane or intracytoplasmic structural domains since it is a glycosylphosphatidylinositol (GPI)-anchored glycoprotein (Ortolan et al. 2002). However, the BST-1 protein also located

in the cytoplasm and nucleus in the ALD-induced cardiac hypertrophy group, according to our immunofluorescence results. Therefore, additional research into how BST-1 penetrates the cytoplasm and nucleus in response to ALD activation is needed to explore. In our study, we found that BST-1 may be a risk factor for cardiac hypertrophy. BST-1 is involved in the pathophysiological processes of various diseases. Previous studies have shown that BST-1 binds to serotonin transporter and integrin b and invokes multiple circuits to control anxiety and depressionlike behaviors (Higashida et al. 2017; Lopatina et al. 2017). The experiment results of Gerasimenko et al. (2017) indicated that BST-1 KO showed social deficits or avoidance behavior in middle-aged male mice. BST-1 KO mice showed depression-like behavior and responded well to antidepressant therapy. BST-1 seems to be a new target for the treatment of cardiac hypertrophy, but it may also affect other physiological and pathological processes in the body during this process. Therefore, further studies are needed to control the balance regulation of BST-1.

In conclusion, the present study has demonstrated that BST-1 can be targeted as a potential treatment for cardiac hypertrophy since it is a positive regulator of pathological myocardial hypertrophy and can regulate myocardial hypertrophy *via* the Ca^{2+}/CaN/NFATc3 pathway.

Authors' contributions. CYL, LF designed the study. YY, LNZ, HJC, SL conducted the experiments. XW, FQH were responsible for model building and data analysis. WDZ, AYL, BZ supplied critical reagents. YY wrote the manuscript. All authors read and approved the final manuscript.

Acknowledgements. The authors wish to thank BZ and LNZ for the excellent technical assistance.

Conflict of interests. The authors declare no conflict of interests.

Funding. The author(s) disclosed receipt of the following financial support for the research, authorship, and/or publication of this article: This work was supported by the National Natural Science Foundation of China (NO.81960315); the Department of Education of Guizhou Province (qianjiaoheKYzi[2021]186, qianjiaoheYJSKYJJ(2020)144); the Guizhou Medical University (I-2017-16) and the Guiyang science and technology department (zhukehetong[2021]43-7). the Guizhou Science and Technology Department (qiankehejichu-ZK[2022] yiban359, qiankehepingtairencai[2018]5779-36).

Availability of data and materials. The data used to support the findings of this study are included within the article.

References

Azibani F, Fazal L, Chatziantoniou C, Samuel JL, Delcayre C (2013): Aldosterone mediates cardiac fibrosis in the setting of hypertension. Curr. Hypertens. Rep. **15,** 395-400 https://doi.org/10.1007/s11906-013-0354-3

Bénitah JP, Perrier E, Gómez AM, Vassort G (2001): Effects of aldosterone on transient outward K+ current density in rat ventricular myocytes. J. Physiol. **537,** 151-160 https://doi.org/10.1111/j.1469-7793.2001.0151k.x

Berridge MJ (2006): Remodelling Ca2+ signalling systems and cardiac hypertrophy. Biochem. Soc. Trans. **34,** 228-231 https://doi.org/10.1042/BST0340228

Doris PA (2017): Genetics of hypertension: an assessment of progress in the spontaneously hypertensive rat. Physiol. Genomics **49,** 601-617 https://doi.org/10.1152/physiolgenomics.00065.2017

Ferrero E, Lo Buono N, Morone S, Parotta R, Mancini C, Brusco A, Giacomino A, Augeri S, Rosal-Vela A, Garcia-Rodriguez S (2017): Human canonical CD157/Bst1 is an alternatively spliced isoform masking a previously unidentified primate-specific exon included in a novel transcript. Sci. Rep. **7,** 15923 https://doi.org/10.1038/s41598-017-16184-w

Finckenberg P, Mervaala E (2010): Novel regulators and drug targets of cardiac hypertrophy. J. Hypertens. **28,** S33-38 https://doi.org/10.1097/01.hjh.0000388492.73954.0b

Frey N, McKinsey TA, Olson EN (2000): Decoding calcium signals involved in cardiac growth and function. Nat. Med. **6,** 1221-1227 https://doi.org/10.1038/81321

Gerasimenko M, Lopatina O, Shabalova AA, Cherepanov SM, Salmina AB, Yokoyama S, Goto H, Okamoto h, Yamammoto Y, Ishihara K, Higashida H (2020): Distinct physical condition and social behavior phenotypes of CD157 and CD38 knockout mice during aging. PLoS One **15,** e0244022 https://doi.org/10.1371/journal.pone.0244022

Gul R, Park DR, Shawl AI, Im SY, Nam TS, Lee SH, Ko JK, Jang KY,Kim D, Kim UH (2016): Nicotinic acid adenine dinucleotide phosphate (NAADP) and cyclic ADP-ribose (cADPR) mediate Ca2+ signaling in cardiac hypertrophy induced by β-adrenergic stimulation. PLoS One **11,** e0149125 https://doi.org/10.1371/journal.pone.0149125

Higashida H, Egorova A, Higashida C, Zhong ZG, Yokoyama S, Noda M, Zhang JS (1999): Sympathetic potentiation of cyclic ADP-ribose formation in rat cardiac myocytes. J. Biol. Chem. **274,** 33348-33354 https://doi.org/10.1074/jbc.274.47.33348

Higashida H, Liang M, Yoshihara T, Akther S, Fakhrul A, Stanislav C, Nam TS, Kim UH, Kasai S, Nishimura T (2017): An immunohistochemical, enzymatic, and behavioral study of CD157/BST-1 as a neuroregulator. BMC Neurosci. **18,** 35 https://doi.org/10.1186/s12868-017-0350-7

Hirata Y, Kimura N, Sato K, Ohsugi Y, Takasawa S, Okamoto H, Ishikawa J, Kaisho T, Ishihara K, Hirano T (1994): ADP ribosyl cyclase activity of a novel bone marrow stromal cell surface molecule, BST-1. FEBS Lett. **356,** 244-248 https://doi.org/10.1016/0014-5793(94)01279-2

Holjak EJB, Savinova I, Nelson VL, Savinova I, Nelson VL, Ogilvie LM, Ng AM, Edgett BA, Platt MJ, Brunt KR, Ask K, Simpson JA (2022): An evaluation of cardiac health in the spontaneously hypertensive rat colony: Implications of evolutionary driven increases in concentric hypertrophy. Am. J. Hypertens. **35,** 264-271 https://doi.org/10.1093/ajh/hpab155

Ishihara K, Hirano T (2000): BST-1/CD157 regulates the humoral immune responses in vivo. Chem. Immunol. **75,** 235-255

https://doi.org/10.1159/000058772
Johnson DB, Dell'Italia LJ (1996): Cardiac hypertrophy and failure in hypertension. Curr. Opin. Nephrol. Hypertens. **5,** 186-191 https://doi.org/10.1097/00041552-199603000-00016
Kakalis LT, Kennedy M, Sikkink R, Rusnak F, Armitage IM (1995): Characterization of the calcium-binding sites of calcineurin B. FEBS Lett. **362,** 55-58 https://doi.org/10.1016/0014-5793(95)00207-P
Koitabashi N, Kass DA (2011): Reverse remodeling in heart failure--mechanisms and therapeutic opportunities. Nat. Rev. Cardiol. **9,** 147-157 https://doi.org/10.1038/nrcardio.2011.172
Lee HC, Aarhus R (1991): ADP-ribosyl cyclase: an enzyme that cyclizes NAD+ into a calcium-mobilizing metabolite. Cell. Regul. **2,** 203-209 https://doi.org/10.1091/mbc.2.3.203
Li H, Rao A, Hogan PG (2011): Interaction of calcineurin with substrates and targeting proteins. Trends Cell Biol. **21,** 91-103 https://doi.org/10.1016/j.tcb.2010.09.011
Li J, Li H, Cai S, Bai S, Cai H, Zhang X (2021): CD157 in bone marrow mesenchymal stem cells mediates mitochondrial production and transfer to improve neuronal apoptosis and functional recovery after spinal cord injury. Stem Cell Res. Ther. **12,** 289 https://doi.org/10.1186/s13287-021-02305-w
Lopatina OL, Furuhara K, Ishihara K, Salmina AB, Higashida H (2017): Communication impairment in ultrasonic vocal repertoire during the suckling period of Cd157 knockout mice: transient improvement by oxytocin. Front. Neurosci. **11,** 266 https://doi.org/10.3389/fnins.2017.00266
Malavasi F, Deaglio S, Funaro A, Funaro A, Ferrero E, Horenstein AL, Ortolan E, Vaisitti T, Aydin S (2008): Evolution and function of the ADP ribosyl cyclase/CD38 gene family in physiology and pathology. Physiol. Rev. **88,** 841-886 https://doi.org/10.1152/physrev.00035.2007
Molkentin JD, Lu JR, Antos CL, Markham B, Richardson J, Robbins J, Grant SR, Olson EN (1998): A calcineurin-dependent transcriptional pathway for cardiac hypertrophy. Cell **93,** 215-228 https://doi.org/10.1016/S0092-8674(00)81573-1
Morone S, Augeri S, Cuccioloni M, Mozzicafreddo M, Angeletti M, Lo Buono N, Giacomino A, Ortolan E, Funaro A (2014): Binding of CD157 protein to fibronectin regulates cell adhesion and spreading. J. Biol. Chem. **289,** 15588-15601 https://doi.org/10.1074/jbc.M113.535070
Nakamura M, Sadoshima J (2018): Mechanisms of physiological and pathological cardiac hypertrophy. Nat. Rev. Cardiol. **15,** 387-407 https://doi.org/10.1038/s41569-018-0007-y
Oldfield CJ, Duhamel TA, Dhalla NS (2020): Mechanisms for the transition from physiological to pathological cardiac hypertrophy. Can. J. Physiol. Pharmacol. **98,** 74-84 https://doi.org/10.1139/cjpp-2019-0566
Ortolan E, Vacca P, Capobianco A, Armando E, Crivellin F, Horenstein A, Malavasi F (2002): CD157, the Janus of CD38 but with a unique personality. Cell. Biochem. Funct. **20,** 309-322 https://doi.org/10.1002/cbf.978
Potter LR, Yoder AR, Flora DR, Antos LK, Dickey DM (2009): Natriuretic peptides: their structures, receptors, physiologic functions and therapeutic applications. Handb. Exp. Pharmacol. **191,** 341-366 https://doi.org/10.1007/978-3-540-68964-5_15
Raman VK, Lee YA, Lindpaintner K (1995): The cardiac renin-angiotensin-aldosterone system and hypertensive cardiac hypertrophy. Am. J. Cardiol. **76,** 18-23 https://doi.org/10.1016/S0002-9149(99)80487-1
Rao A (2009): Signaling to gene expression: calcium, calcineurin and NFAT. Nat. Immunol. **10,** 3-5 https://doi.org/10.1038/ni0109-3
Samak M, Fatullayev J, Sabashnikov A, Zeriouh M, Schmack B, Farag M, Popov AF, Dohmen PM, Choi YH, Wahlers T, Weymann A (2016): Cardiac hypertrophy: An introduction to molecular and cellular basis. Med. Sci. Monit. Basic Res. **22,** 75-79 https://doi.org/10.12659/MSMBR.900437
Somanna NK, Yariswamy M, Garagliano JM, Siebenlist U, Mummidi S, Valente AJ, Chandrasekar B (2015): Aldosterone-induced cardiomyocyte growth, and fibroblast migration and proliferation are mediated by TRAF3IP2. Cell. Signal. **27,** 1928-1938 https://doi.org/10.1016/j.cellsig.2015.07.001
Takano APC, Senger N, Barreto-Chaves MLM (2020): The endocrinological component and signaling pathways associated to cardiac hypertrophy. Mol. Cell. Endocrinol. **518,** 110972 https://doi.org/10.1016/j.mce.2020.110972
Tham YK, Bernardo BC, Ooi JY, Weeks KL, McMullen JR (2015): Pathophysiology of cardiac hypertrophy and heart failure: signaling pathways and novel therapeutic targets. Arch. Toxicol. **89,** 1401-1438 https://doi.org/10.1007/s00204-015-1477-x
van Rooij E, Doevendans PA, de Theije CC, Babiker FA, Molkentin JD, de Windt LJ (2002): Requirement of nuclear factor of activated T-cells in calcineurin-mediated cardiomyocyte hypertrophy. J. Biol. Chem. **277,** 48617-48626 https://doi.org/10.1074/jbc.M206532200
Yamamoto-Katayama S, Ariyoshi M, Ishihara K, Hirano T, Jingami H, Morikawa K (2002): Crystallographic studies on human BST-1/CD157 with ADP-ribosyl cyclase and NAD glycohydrolase activities. J. Mol. Biol. **316,** 711-723 https://doi.org/10.1006/jmbi.2001.5386
Yamazaki T, Komuro I, Yazaki Y (1999): Role of the renin-angiotensin system in cardiac hypertrophy. Am. J. Cardiol. **83,** 53-57 https://doi.org/10.1016/S0002-9149(99)00259-3
Zarain-Herzberg A, Fragoso-Medina J, Estrada-Avilés R (2011): Calcium-regulated transcriptional pathways in the normal and pathologic heart. IUBMB Life **63,** 847-855 https://doi.org/10.1002/iub.545
Zeitz MJ, Smyth JW (2020): Translating translation to mechanisms of cardiac hypertrophy. J. Cardiovasc. Dev. Dis. **7,** 9 https://doi.org/10.3390/jcdd7010009
Zhang Q, Qi H, Cao Y, Cao Y, Shi P, Song C, Ba L, Chen Y, Gao J, Li S, et al. (2018): Activation of transient receptor potential vanilloid 3 channel (TRPV3) aggravated pathological cardiac hypertrophy via calcineurin/NFATc3 pathway in rats. J. Cell. Mol. Med. **22,** 6055-6067 https://doi.org/10.1111/jcmm.13880

Received: September 15, 2022
Final version accepted: November 30, 2022